European Journal of Remote Sensing

ISSN: (Print) 2279-7254 (Online) Journal homepage: http://www.tandfonline.com/loi/tejr20

Assessment of Regional Shallow Landslide Stability Based on Airborne Laser Scanning Data in the Yingxiu Area of Sichuan Province (China)

Chun Liu, Min Hu, Ping Lu, Weiyue Li, Marco Scaioni, Hangbin Wu, Yu Huang & Bin Ye

To cite this article: Chun Liu, Min Hu, Ping Lu, Weiyue Li, Marco Scaioni, Hangbin Wu, Yu Huang & Bin Ye (2016) Assessment of Regional Shallow Landslide Stability Based on Airborne Laser Scanning Data in the Yingxiu Area of Sichuan Province (China), European Journal of Remote Sensing, 49:1, 835-860

To link to this article: http://dx.doi.org/10.5721/EuJRS20164944

Published online: 17 Feb 2017.

European Journal of Remote Sensing - 2016, 49: 835-860
doi: 10.5721/EuJRS20164944
Received 11/04/2016 accepted 20/11/2016

European Journal of Remote Sensing
An official journal of the Italian Society of Remote Sensing

www.aitjournal.com

Assessment of Regional Shallow Landslide Stability Based on Airborne Laser Scanning Data in the Yingxiu Area of Sichuan Province (China)

Chun Liu[1], Min Hu[2], Ping Lu[1]*, Weiyue Li[3], Marco Scaioni[4], Hangbin Wu[1], Yu Huang[5] and Bin Ye[5]

[1]College of Surveying and Geo-Informatics, Tongji University, Siping Road 1239, 200092, Shanghai, China
[2]Shanghai Surveying and Mapping Institute, Wuning Road 419, 200063, Shanghai, China
[3]Institute for Urban Studies, Shanghai Normal University, Guilin Road 100, 200234, Shanghai, China
[4]Department Architecture, Built Environment and Construction Engineering, Politecnico di Milano, Via G. Ponzio, 31, 20133, Milano, Italy
[5]Department of Geotechnical Engineering, College of Civil Engineering, Tongji University, Siping Road 1239, 200092, Shanghai, China
*Corresponding author, e-mail address: luping@tongji.edu.cn

Abstract

This study focuses on analyzing the slope stabilities in a landslide-prone area of Yingxiu Town, Sichuan Province (China). Airborne Laser Scanning (ALS) data were acquired to derive a Digital Elevation Model (DEM) with sufficient accuracy and resolution, as an input for the regional landslide stability analysis. The one-dimensional hydrological model - Stability Index Map (SINMAP), functioning with topographic data, geological settings, and rainfall conditions, was used as a simplified model for slope stability mapping. In this study, the investigated region was classified into six stability levels, and data reliability was subsequently checked with reference to recent landslide inventories. Several experiments have shown that the quality of ALS data played a key-role in the slope stability inside the SINMAP model regarding the point cloud density and the random error. Higher point cloud density may construct higher precision of DEM, however, it may also produce more noises. Although with these uncertainties, using ALS data and its derived high precision DEM, the physically-based SINMAP model is expected to provide a solid basis for further landslide susceptibility mapping at regional scale.

Keywords: Slope Stability, Airborne Laser Scanning, Stability Index Map (SINMAP), landslides.

Introduction

During last decades, landslides have caused great human and economic losses in southwestern China. Yingxiu is one of the most critical areas that were affected by shallow landslides [Cui et al., 2009, 2011; Xu et al., 2009; Gorum et al., 2011]. In particular, the

"5.12" Wenchuan Earthquake (Ms = 8.0; epicenter at 31.0°N, 103.4°E) that struck this area on May 5, 2008, weakened and loosened the structural settings at regional scale, consequently increasing the landslide occurrences due to intensive rainfall [Cui et al., 2009; Xu and Xu, 2013].

Effective approaches for evaluating and predicting runoff distances of shallow landslides are urgently needed from social, environmental, and economic perspectives in the Yingxiu area. Recently, abundant slope stability studies have been conducted based on various methods, spanning from geological field surveys to remote-sensing techniques based on data collected from satellites and aerial vehicles [Lu et al., 2011; Li et al., 2016], aircrafts and Unmanned Aerial Vehicles (UAV, Turner et al. [2015], SAR Interferometry [Lu et al., 2010, 2012, 2014a] and spatial sensor network [Qiao et al., 2013; Lu et al., 2015a].

Topographic data representing slopes potentially affected by shallow landslides are particularly important if sufficient spatial resolution and accuracy can be achieved. In general, Digital Elevation Models (DEM) can be derived from photogrammetric data processing of optical images and from laser scanning point clouds. Nevertheless, photogrammetry is a passive technique that may be strongly influenced by the quality of sunlight and surface texture. In contrast, Light Detection and Ranging (LiDAR) is an active technique and the measurement process is nearly independent of the weather conditions and acquisition time. These properties are important when the measurement operates in rainy and cloudy mountainous areas, such as those slopes in the Yinxiu area. The implementation of LiDAR sensors on airborne platforms and the integration of geo-position sensors (Airborne Laser Scanning, ALS) is able to provide a reliable DEM that can be used for regional investigation with accuracy (horizontal and vertical) and spatial resolution at sub-meter level [Sekiguchi and Sato, 2004; Reutebush et al., 2005]. The accuracy and spatial resolution are better than those products generated from conventional topographic methods [Jaboyedoff et al., 2012]. Therefore, ALS generally has more advantages than photogrammetry for producing decent resolution DEM. Also, ALS does not require texture data, offers nearly instantaneous availability of the digital model (no heavy post-processing required) and is operational during the day/night and under weather conditions that are not favourable for photogrammetry. All of these key-points are important when considering landslide stability analysis applications.

After DEM construction, a suitable model is required for landslide stability analysis. Recently, most researchers have used statistical and physically-based models to investigate shallow landslides [Hong et al., 2015; Lu et al., 2014b, 2015b]. Statistical models can also derive their predictions from external observations of triggering factors [Carrara et al., 1991; Lee, 2005]. However, most parameters are subjective and difficult to be quantitatively measured in the field. Physically-based models are advantageous because they also consider physical landslide mechanisms. Therefore, preference was given to the popular physically-based model of Stability Index Map [SINMAP, Pack et al., 1998], which can be well implemented in a Geographical Information System (GIS) environment.

The GIS-based SINMAP model is a simplified infinite slope stability model that incorporates a topography-based hydrological model TOPMODEL [Hammond et al., 1992; Beven et al., 1995]. This model can accommodate uncertain soil density, cohesion, and internal friction

values using a uniform probability distribution. This model requires a precise DEM, which can be precisely estimated from LiDAR data. The SINMAP model can quickly identify hazardous regions and provide a detailed assessment based on relatively coarse information. This method reduces the difficulties associated with data acquisition in harsh environments, such as in mountainous regions. In addition, landslide risk can be further assessed using the SINMAP model combining with remote sensing and GIS data. A stability index (SI) can be defined and evaluated to determine the slope stability levels based on different safety factor (FS) values. The output slope stability map can be used later as a tool for land use planning, landslide hazard management and risk governance. This can be usually implemented within the GIS environment [Van Western, 2000].

In this study, the slope stability of the landslide-prone Yingxiu region in Sichuan Province of China was investigated using ALS data and the SINMAP model. This paper includes a brief presentation of the Yingxiu study area, an introduction of the ALS data acquisition and processing, a description of the slope stability analysis, and derived results and discussion.

Study area

The Yingxiu area is located in Sichuan Province, China (red rectangle in Fig. 1), and covers a total area of 142.20 km2. Five administration units are included: Yinxing Village (A), the town of Yingxiu (B), Baihua Village (C), the town of Xuankou (D) and Dujiangyan City (E). From a geological perspective, the materials in the region are generally characterized as loose soils with silt and clay textures, and the exposed lithology mainly consists of sandstone, diorite, biotite, granite, and granodiorite, with rock fissures due to weathering that facilitate water infiltration [Chen et al., 2011]. According to the local geological hazards investigation report in 2005 [Yang et al., 2005], the annual average precipitation is about 1,285.1 mm. The Minjiang River, which is bordered by steep mountains, corresponds to the main surface flow in the region. Prolonged groundwater circulation and river erosion likely create ideal conditions for shallow runoff, which may bring an unstable region with frequent landslides and debris flows. Moreover, this region was strongly shocked by the “5.12” Wenchuan earthquake in 2008, which generated a 250-km surface rupture along the Yingxiu-Beichuan fault system (green dashed line in Fig. 1) that exactly crosses the study area. After the Wenchuan earthquake, the number of landslide occurrences and their related casualties significantly increased, largely due to changes in the geological structure, which decreased the slope stability. During the rainy season, the Yingxiu area suffers annually from landslide disasters that affect residents, properties, and infrastructures [Tang et al., 2011]. As a result, considerable economical investments and resources have been used to investigate geo-disasters and identify landslide-prone areas in this region.

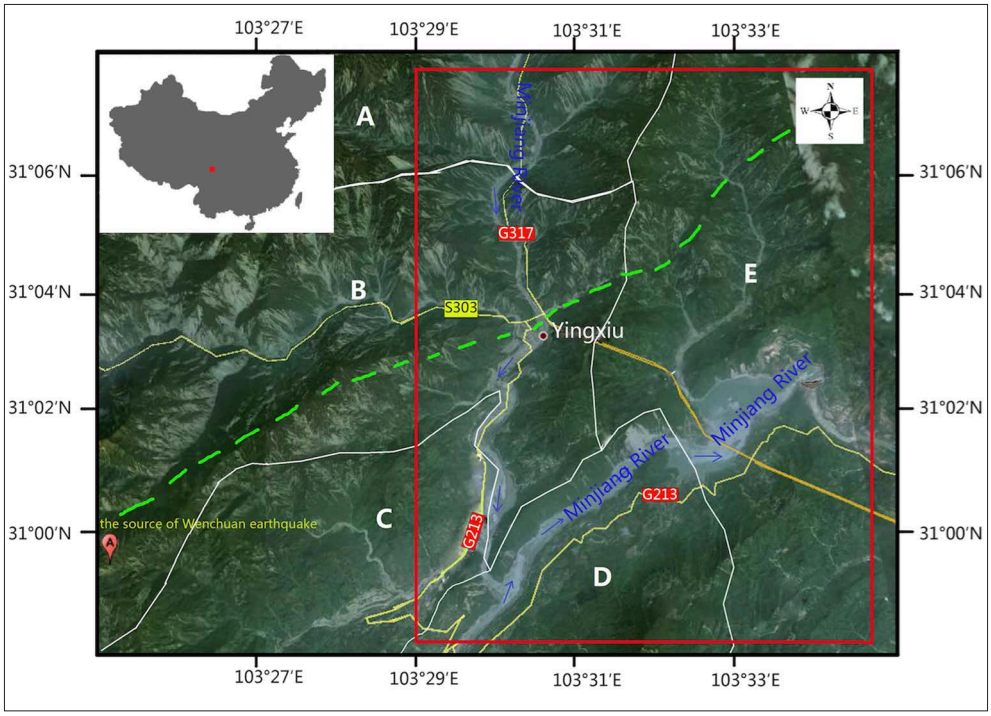

Figure 1 - The study area. The red rectangle encloses the Yingxiu area in Sichuan Province (China). The green dashed line represents the surface rupture after the "5.12" Wenchuan earthquake. This background image was obtained from Google Earth® on April 11, 2011, with a spatial resolution of 30 m.

Methodology

ALS data acquisition and processing

ALS data acquisition

The ALS flight mission was performed to optimize the quality of topographic data in the Yinxiu area. The most critical aspect of the project was related to the presence of relief and steep slopes in this region, which may achieve a non-homogenous ALS data resolution. The aerial LiDAR flight scheme consisted of several overlapping flight lines that covered the entire region. The average overlap between adjacent strips was designated as 30%. The flight height was approximately 2500 m a.s.l., and the ALS data were collected using a Leica ALS70 sensor. The mission was accomplished on 29 August 2009, about 15 months after the Wenchuan earthquake. A point cloud of 8.5 billion elevation points covering an area of approximately 142.20 km^2 was obtained. Multi-echo returns were recorded and archived. The point cloud data included ground, vegetation, and building points, with a slightly lower density in the vegetated areas than that in the open areas because of the higher variations in local height. The average point distribution was about 6 points /m^2, which was sufficient for describing the topographical features and earthquake-induced changes. Filtering of non-terrain points was conducted using the Terrasolid® software, version 013.006.

ALS data processing

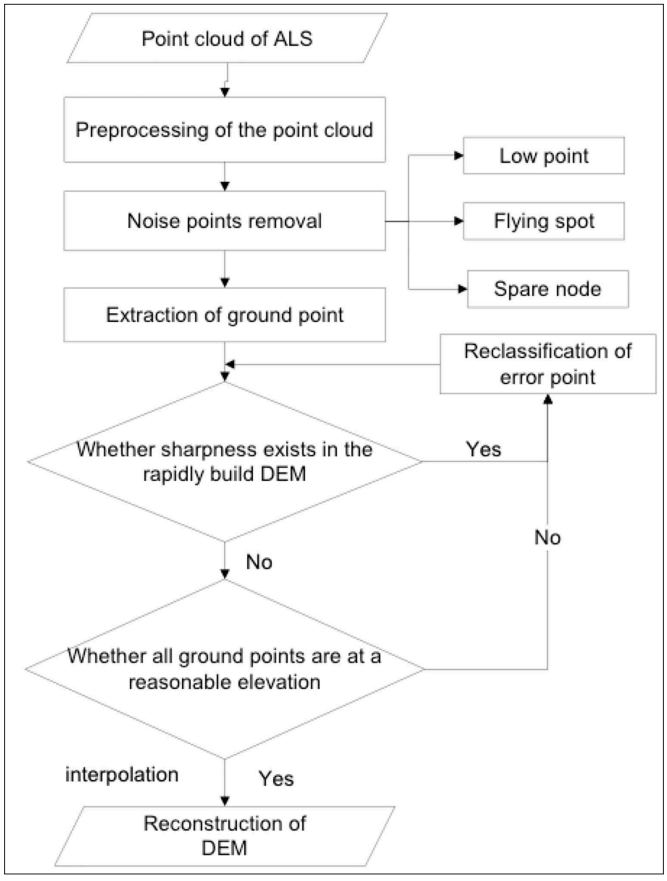

Figure 2 - The flow chart of the ALS data processing.

The acquired ALS point cloud data were processed with four steps: (1) pre-processing; (2) noise filtering; (3) ground-point extraction and (4) result validation (see the detailed workflow in Fig. 2). During the first step, the ALS data were checked to determine their quality and the correctness of the attributes, such as the coordinate system, flight information, and other metadata. Several noisy regions were observed in the LiDAR datasets, which were probably due to multipath measurement errors, flying spots caused by the reflection of low-flying objects, and spare nodes. The second step was mainly based on the height algorithm, which compares the local elevation of the centre point with other points in a local neighbourhood. The remaining points after filtering represented the actual object points that were captured over vegetation, buildings and the ground. Considering that only ground points were needed for DEM construction in the third step, the extraction was accomplished by using the Triangulated Irregular Network (TIN) filtering method [Axelsson, 2000]. This method consists of the following three steps: (1) choosing lower elevation points to build the TIN, (2) iteratively filtering new ground laser points over the TIN based on distance and angle, with each additional surface point approximating the

model to reality, and (3) classification of ground points according to the ground type. After extraction, the removed points were checked by comparing themselves with the DEM and by statistical analysis of the residuals. On one hand, the DEM smoothness was analyzed under the assumption that any local elevation gaps could indicate some non-ground points that were correctly eliminated. On the other hand, this analysis ensured that all values were within a reasonable elevation range. For example, Z values could not be negative or one million, and should correspond to the height of the area. After the processing of the ALS point cloud, the average density of the final ground point was 2 points /m^2. These ground points were used to construct a 10 x 10 m grid DEM based on the standard Kriging interpolation.

As mentioned in Section "Intoduction", ALS data are generally suitable for producing high-resolution DEM in mountainous regions. However, several limitations may be involved in this process. First, several systematic errors may occur, such as errors due to system calibration, geo-referencing, strip alignment and merging, and missing data. Second, the amount of ALS data may be large, which can result in longer processing times and call for high-performance computers. Third, the quality of the final slope stability map depends directly on data filtering. If the adopted filtering algorithm does not work properly, the DEM will not represent the actual terrain and the final slope instability evaluation will introduce bias.

The SINMAP model

Theory

Geological characteristics of terrain are one of the main factors that control landslide occurrence. However, the Yingxiu area is large and does not allow a detailed consideration of all geological data. The SINMAP model is particularly suitable for coping with this problem because it combines hydrological conditions, geological data and topography. Hydrological conditions are very important for triggering shallow landslides because rainfall and groundwater circulation may influence the soil moisture and cause flow convergence in catchments where landslides frequently occur. Thus, in the SINMAP model, the 'specific catchment area' (a) is defined as the upslope contributing area of the catchment per unit of contour length [m^2/m] (Fig. 3). This parameter is closely tied to hydrological models that represent runoff generation as saturation from below [Beven and Kirby, 1979; O'loughlin, 1986; Moore and O'loughlin, 1988; Moore and Grayson, 1991]. To evaluate the water contribution, a wetness index (w) is calculated based on the TOPMODEL theory [Beven and Kirby, 1979]:

$$w = \min\left(\frac{Ra}{T\sin\theta}, 1\right) \quad [1]$$

where R is the threshold value for landslide triggering [m/h], T is the soil transmissivity [m^2/h], a is the specific catchment area [m], and θ is the slope angle. The R/T [m^{-1}] ratio combines both climate and hydrogeological factors. The wetness index w has an upper boundary of 1.

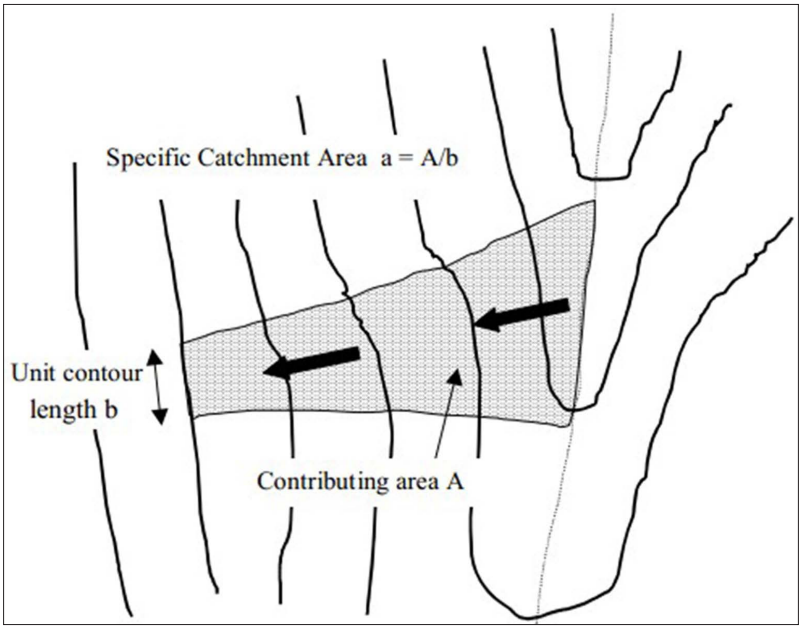

Figure 3 - Definition of the specific catchment area as proposed by Reutebush et al., 2005.

The SINMAP model [Reutebush et al., 2005] is based on the infinite slope stability [Hammond et al., 1992] and the hydrological theories [Dietrich et al., 1995], with a factor safety (*FS*) defined as follows:

$$FS = \frac{C + \cos[1 - wr]\tan\varphi}{\sin\theta} \quad [2]$$

where $r=\rho_w/\rho_s$ is the density ratio between the water and soil (ρ_w and ρ_s [kg/m^3], respectively), φ is the internal friction angle of the soil, and *D* is the vertical soil depth [m]. *C* corresponds to the dimensionless combined cohesion, which is computed from the root cohesion (C_r) and soil cohesion (C_s) as follows:

$$C = (C_r + C_s) / D\cos\theta\rho_s g \quad [3]$$

where *g* is the gravitational acceleration (9.81 m/s^2) and Eqs. [2] and [3] were combined to obtain the *FS* as follows:

$$FS = \frac{C + \cos\theta[1 - \min\left(\frac{Ra}{T\sin\theta}, 1\right)r]\tan\varphi}{\sin\theta} \quad [4]$$

Theoretically, when $FS > 1$ the slope is considered stable and when $FS \leq 1$ the slope is considered unstable. In practical applications, the input parameters cannot be properly evaluated for several reasons, including uncertainties of direct and indirect measurements, the necessary model approximations that are needed to define parameters in Equation [4], and the uneven geotechnical conditions in the investigated region. To cope with this problem, the SINMAP model allows variability in cohesion, internal friction angle, and R/T ratio by using a uniform probability distribution in a specified domain. According to various combinations of maximum and minimum values for the input parameters, two extreme values of FS (FS_{min} and FS_{max}) were calculated and implemented to define the stability index (SI), which determines the slope stability as follows:

$$SI = \begin{cases} FS_{\min} & (FS_{\min} > 1, FS_{\max} > 1) \\ \Pr ob & (FS > 1)(FS_{\min} < 1, FS_{\max} > 1) \\ 0 & (FS_{\max} < 1) \end{cases} \quad [5]$$

Equation [5] shows that three independent calculation processes were used to calculate the SI according to the maximum and minimum FS. Six safety classes were defined according to the SI value (Tab. 1). From class 1 to 3 the slope can be considered unstable, and the other classes represent different degrees of stability.

Table 1 - The classification of slope stability according to the stability index (SI) calculated from the SINMAP model.

Condition	Class	Predicted state
$SI = 0$	1	High instability
$0.5 \geq SI > 0$	2	Medium instability
$1.0 \geq SI > 0.5$	3	Low instability
$1.25 \geq SI > 1.0$	4	Quasi-stable slope
$1.5 \geq SI > 1.25$	5	Moderately stable slope
$SI > 1.5$	6	Stable slope

Data collection and processing

The geotechnical properties of the soils in the study area [Chen et al., 2011] are shown in Table 2. These values were derived from published reports and inverse modelling. The rock type was organized in 12 classes, depending on the rock layer attributes (Fig. 4). The main rock type of the study area is composed of Lithic quartz sandstone, siltstone, mudstone with conglomerate and marl, mainly medium-fine biotite adamelli in the North, and sand gravel along the Minjiang River. The maximum and minimum values for all types were calculated for the entire region.

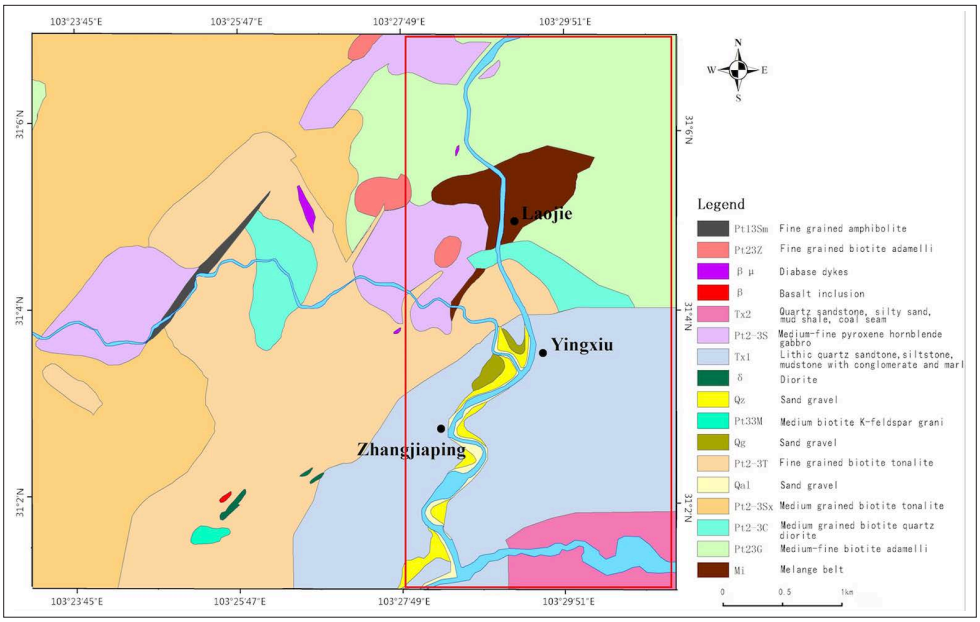

Figure 4 - The map of rock types modified after Chen et al. [2011] (red rectangle encloses the study area).

Although rainfall is assumed to be a triggering factor for shallow landslides, no consensus exists regarding a threshold value for this study area. Consequently, the maximum alert value for the 2001-2013 rainy season was selected based on the news in the media and the geological hazard investigation report. The rainfall lasted more than 12 hours and the cumulative precipitation reached 105.2 mm, which triggered a number of landslides. Therefore, the rainfall intensity of 8.76 mm/h was selected as the maximum alert threshold for landslide occurrence [Yang et al., 2005].

Table 2 - Geotechnical parameters of the study area.

Data	Parameter	Symbol	Source	Value	Unit
Geotechnical parameters	Cohesion	C	[Chen et al., 2011][19]	3400, 4000	N/m^2
	Internal friction angle	φ		30, 55	Degree
	Unit weight of soil	γ		21500, 22000	N/m^3
	Soil transmissivity	T		0.072, 0.875	m^2/h
Rainfall	Rainfall	R	2005 local geological hazards investigation report [20] and recent news	8.76	mm/h
Recent data	Landslide location	-	-	-	-
Topography	Slope	θ	ALS data	-	Degree
	Specific catchment area	a		-	m

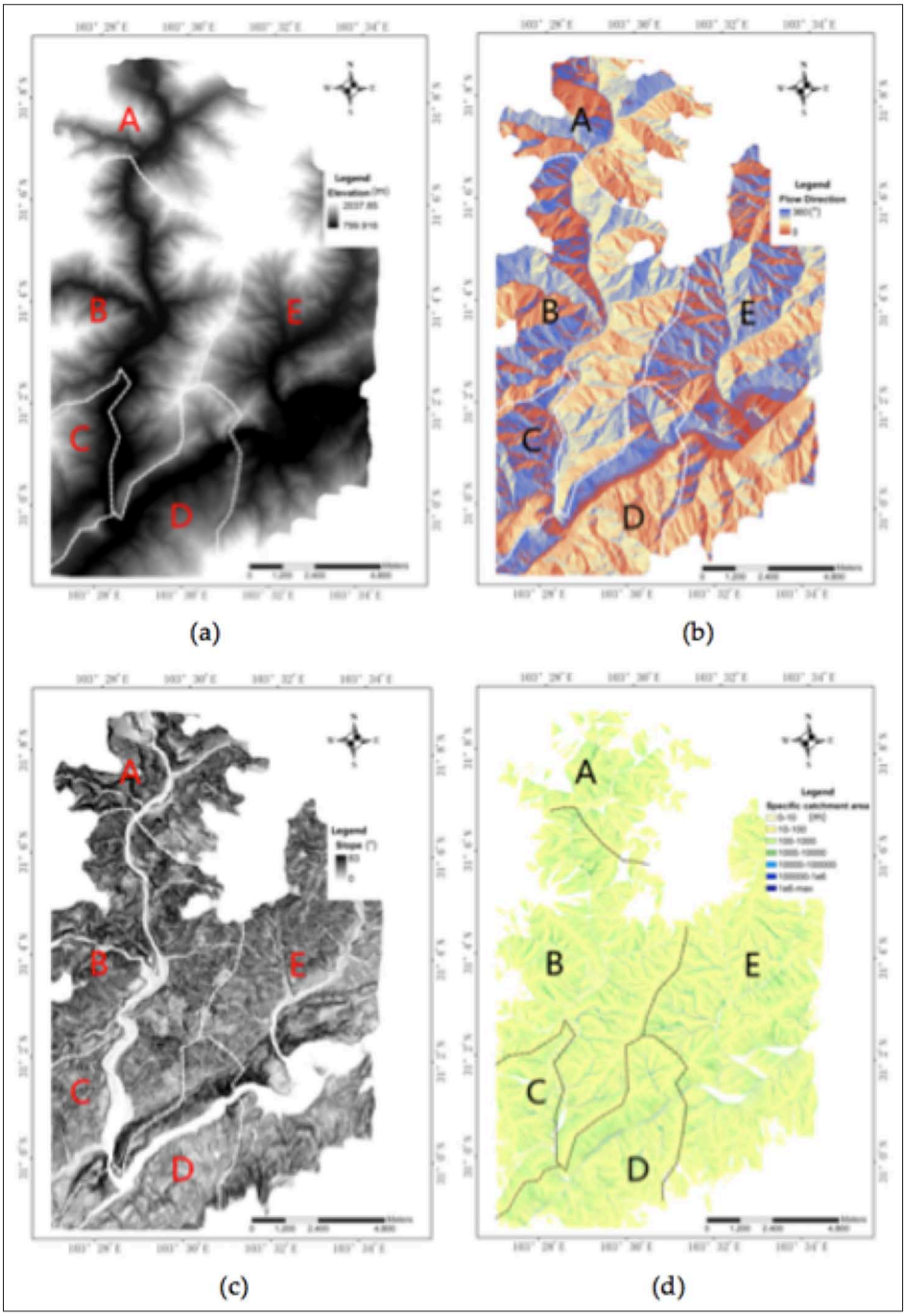

Figure 5 - Four maps used as inputs for the SINMAP model: (a) the pit-filled DEM; (b) the water-flow direction map; (c) the slope angle map; (d) the specific catchment area map.

The open-source code SINMAP 2.0 (http://hydrology.usu.edu/sinmap2/) developed by Utah State University [Logan, Utah, USA] was implemented in this study. This code can be run as a plug-in in ArcGIS. The four raster maps derived from the LiDAR DEM were used as input for the SINMAP model (Fig. 5): (1) the pit-filled DEM map, (2) the slope angle map, (3) the water-flow direction map and (4) the specific catchment area map.The elevation in the study ranges from 799 m to 2027 m a.s.l., and the maximum slope angle is 83°. The water-flow direction (ranging from 0–2π) represents the compass direction of the flow, and the angle of the direction is defined in a counter-clockwise direction from the East. The specific catchment area is divided in seven classes using intervals based on powers of 10 (i.e., 1, 10, 10^2, …, 10^6). This parameter represents the drainage network. The raster maps, geotechnical parameters and rainfall rates have been chosen as input parameters in SINMAP 2.0 to calculate the final slope stability map. A safety index (*SI*) ranging from 0-10 was computed for each raster cell of 10 × 10 m^2. Then, the ESRI ArcGIS software (version 9.3) was used to transform the cloud of irregularly spaced elevation points to a regular 10m grid as a trade-off between the SINMAP requirements and the computational effort.

Results and discussion

Relationship between terrain and landslide occurrence

When compared with the image from Google Earth (Fig. 1), the three-dimensional DEM appears to provide a reliable reproduction of the actual terrain characteristics (Fig. 6). An inventory of recent shallow landslides data was collected during 2008-2013 (Tab. 3). Each event is described by its geographic location and two attributes (name and time of occurrence). Most landslides were triggered by precipitation during June-August, with significant higher frequencies along the National Road 213, the Highway 31, and the town of Xuankou. Most of the landslides occurred in the north of the Yingxiu area, which is known as a typical landslide-prone region (Fig. 6). The DEM revealed a concentration of landslides that occurred in steep mountains along the Minjiang River, with several events located at the mountain toe, which is easily eroded by long-term river scouring. Other landslides occurred in the middle of mountain slopes or near the mountaintops where the gradient is relatively steeper. These slopes corresponded to inner gorges or valleys [Kelsey, 1988; Chigira et al., 2010]. The presence of many main roads along the Minjiang Valley may explain why nearly half of the landslides occurred there. Indeed, road cuts are significant predisposing factors for triggering landslides. In addition, topography as well as other geographic conditions (for example, the proximity to rivers), plays an important role in the development of shallow landslides.

Table 3 - Inventory of the recently-occurred shallow landslides in the Yingxiu area.

Name	ID	Date (MM/DD/YY)	Longitude	Latitude
Yingxiu	1	7.1.2008	103°29’30.29”E	31°4’16.01”N
	2	7.1.2008	103°29’27.31”E	31°4’7.42”N
	3	7.1.2008	103°29’28.21”E	31°4’5.07”N
	4	7.1.2008	103°29’38.24”E	31°3’33.82”N
Zaojiaowan tunnel	5	8.14.2010	103°29’19.59”E	31°7’19.35”N
	6	8.14.2010	103°29’12.98”E	31°7’9.29”N
National road 213	7	8.14.2010	103°28’28.77”E	31°6’8.32”N
	8	8.14.2010	103°28’49.14”E	31°6’14.85”N
	9	8.14.2010	103°29’29.47”E	31°5’26.80”N
	10	8.14.2010	103°29’10.51”E	31°5’22.72”N
	11	8.15.2010	103°29’14.88”E	31°6’5.25”N
	12	6.9.2013	103°29’24.54”E	31°5’52.21”N
	13	6.9.2013	103°28’8.88”E	31°5’47.64”N
	14	7.23.2013	103°29’0.97”E	31°5’53.32”N
Highway 31	15	8.14.2010	103°27’32.01”E	31°4’58.05”N
	16	7.1.2011	103°28’41.77”E	31°4’16.19”N
	17	7.1.2011	103°28’18.96”E	31°4’13.70”N
	18	7.4.2011	103°29’0.69”E	31°4’1.63”N
	19	7.4.2011	103°28’48.27”E	31°4’0.57”N
Xuankou	20	8.15.2010	103°28’43.15”E	31°0’1.72”N
	21	8.15.2010	103°28’4.91”E	30°59’31.23”N
	22	8.15.2010	103°28’1.01”E	30°59’26.50”N
	23	8.15.2010	103°27’35.37”E	30°59’39.03”N
	24	8.15.2010	103°27’28.00”E	30°59’22.85”N
Dujiangyan City	25	6.9.2013	103°32’59.73”E	31°2’28.72”N
	26	6.9.2013	103°33’11.44”E	31°2’32.45”N
	27	6.9.2013	103°30’24.54”E	31°2’52.21”N
Minjiang River	28	7.4.2011	103°28’2.17”E	31°1’53.68”N
Duwen highway	29	6.9.2013	103°31’56.04”E	31°2’23.29”N
Yinxing	30	7.1.2008	103°28’6.74”E	31°7’35.16”N
	31	7.1.2008	103°28’12.91”E	31° 8’25.32”N
Zhangjiaping	32	7.4.2011	103°27’53.19”E	31°2’34.29”N

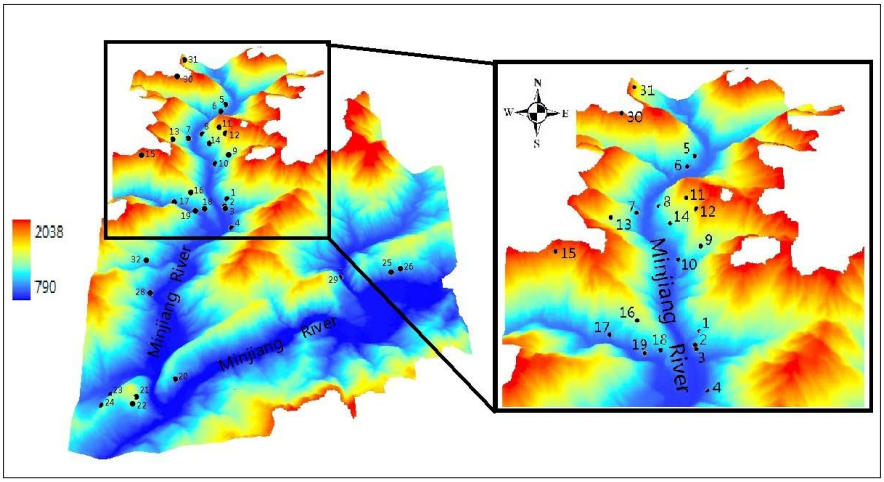

Figure 6 - A three-dimensional representation of the terrain for the study area (black dots showing the landslide occurrences that mentioned in Tab. 3).

Slope stability distribution

According to the stability levels listed in Table 1, the study area was classified into six categories from unstable to stable. Table 4 shows the extension of each safety class, and the spatial distributions of each class can be found in Figure 7. Here, the unstable areas are characterized as red (class 1), orange (class 2), and yellow (class 3) zones. In addition, purple circles were used to highlight the areas of highest hazard (class 1). By overlaying a layer that reproduces human settlements in the same region, the slope stability map can be used to identify high risky areas for inhabitants and infrastructures. The human settlement maps include parts of the administrative units of the Yinxing Village, the towns of Yingxiu and Xuankou, and Dujiangyan City (purple triangular points in Fig. 7). Some points, such as those for the town of Yingxiu and Xuankou Village, were within the unstable region predicted by the SINMAP model, which indicated the need for additional protection measurements in these areas.

The unstable regions (lower SI) accounted for 14.43% of the total area, while the stable regions accounted for 85.57% (Tab. 4). The red and orange zones are mainly located in the northwest of the study area and near the regional boundary, and the remaining zones are mostly located on the steep mountains in the south along the Minjiang River. The terrains in those stable areas (identified as cyan (class 4), blue (class 5), and aqua (class 6) zones) are flat and far away from the river. To understand the frequently landslide occurrences along the riverside, further studies analyzing the detailed river profiles may be needed to deeply investigate the influence of active tectonics [Lu and Shang, 2015]. The landslide occurrences may also be associated with regional active tectonics since river profiles may be tightly associated with active tectonics. By analyzing the slope stability, it may conclude that topography and slope are the main factors that influence the landslide occurrence in this study area when the amount of rainfall was considered to be similar over the entire region.

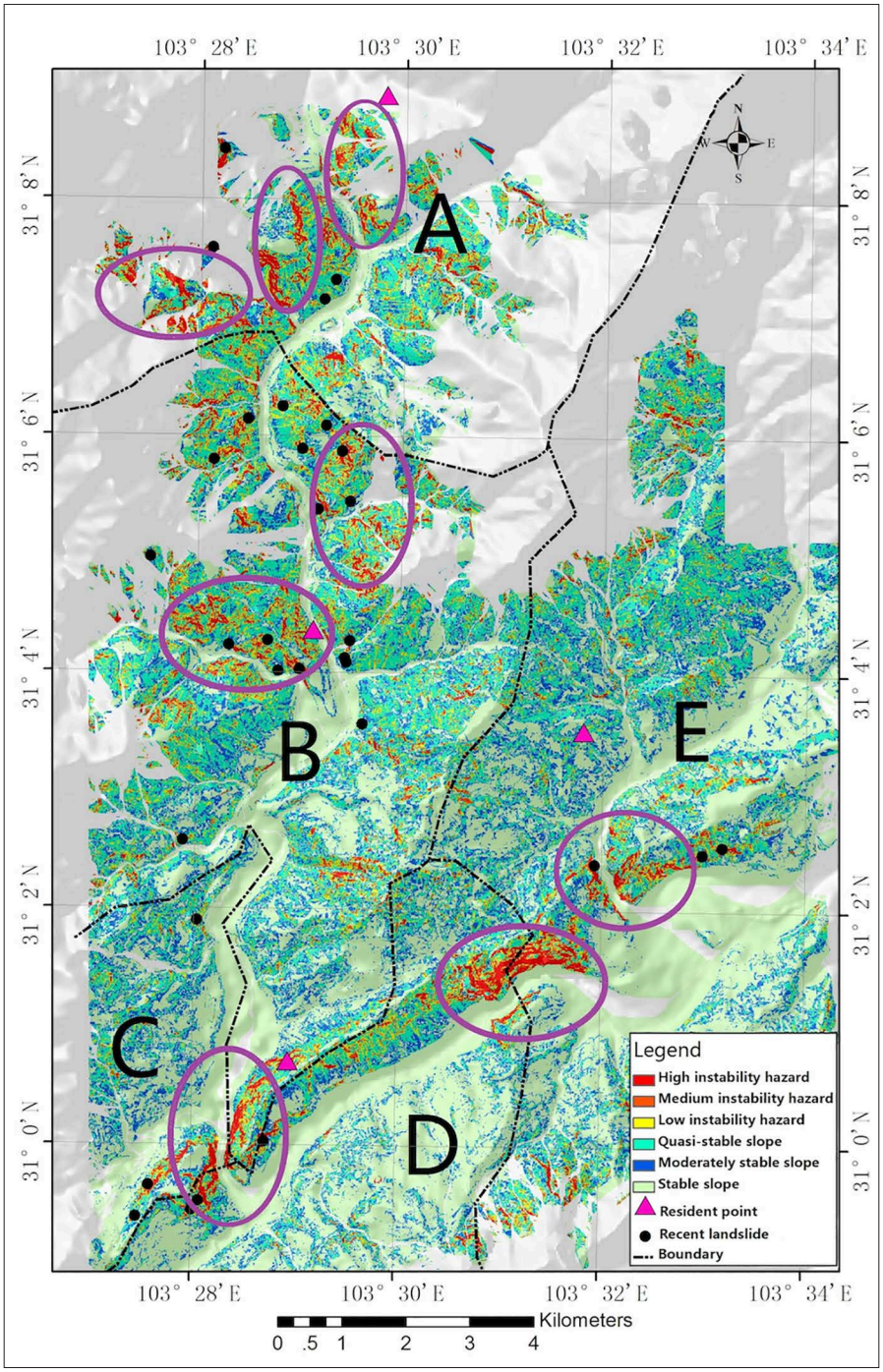

Figure 7 - Slope stability map of the study area produced using the SINMAP model (the purple circles show the areas of highest landslide hazard level).

Table 4 - Statistical summary of the slope stability analysis of the study area.

	Area (km^2), Percentage (%)	Landslide number, Percentage (%)	Landslide density (num/km^2)
High instability	4.06, 2.86%	13, 40.62%	3.20
Medium instability	5.08, 3.57%	4, 12.50%	0.79
Low instability	11.38, 8.00%	9, 28.13%	0.79
Quasi-stable slope	35.93, 25.27%	4, 12.50%	0.11
Moderately stable slope	24.76, 17.42%	2, 6.25%	0.08
Stable slope	60.96, 42.88%	0, 0%	0

Slope stability distribution

The outcomes from both studies confirmed that the northwest region of the Yingxiu area is more susceptible to shallow landslides. To validate this conclusion, 32 recent landslides (indicated by black points in Fig. 7) were overlapped with the slope stability map. The result confirmed that previous events were mainly located in the northwest region of the Yingxiu area, classifying the area as having a higher collapse risk. Twenty-six recent landslides (81.25%) occurred in the regions were classified as unstable in the present study (see Tab. 4). Furthermore, the high instability hazard (class 1) features the highest density of past landslides, and the landslide density decreases from the unstable to stable zones [Sarkar and Kanungo, 2004; Bijukchhen et al., 2013]. The fractions of landslide occurrence in each class also validated the results obtained from this study. In fact, the area with the highest instability hazard (2.86% of the total) contained 40.62% of past landslides (see Tab. 4). However, the landslide occurrence fraction in the low instability hazard zone is greater than that in the medium instability hazard zone. This controversial result could be motivated by the existence of other triggering factors that have not been considered by the SINMAP model, for example, possible mineral exploitation and land use. The landslide record focuses on the following three regions: the boundary between Yinxing Village and the town of Yingxiu, the center of the town of Yingxiu, and the boundary between the towns of Yingxiu and Xuankou. In addition, the reliability of the validation process may depend on the geo-positional accuracy of previous events. In some cases, such accuracy may suffer from the approximations used in the coordinate transformations, geo-referencing errors, etc. On the other hand, the precision of landslide locations is important for SINMAP predictions.

After the conclusion that the results obtained from the SINMAP model at the regional level agree with the results of a previous study and are consistent to landslide inventory data, a more detailed analysis will be conducted to achieve a more complete understanding. Nevertheless, the high instability hazard was calculated using a combination of upper and lower input parameter limits. When the combined values do not reach a stable condition, the slope was defined as a high instability hazard zone. Under such conditions, bare slopes or slopes devoid of soil cover may lead to erroneous results; in this case, the results calculated by the SINMAP model will not be reliable [Terhorst and Kreja, 2009; Deb and El-Kadi, 2009].

Comparison with recent landslide data

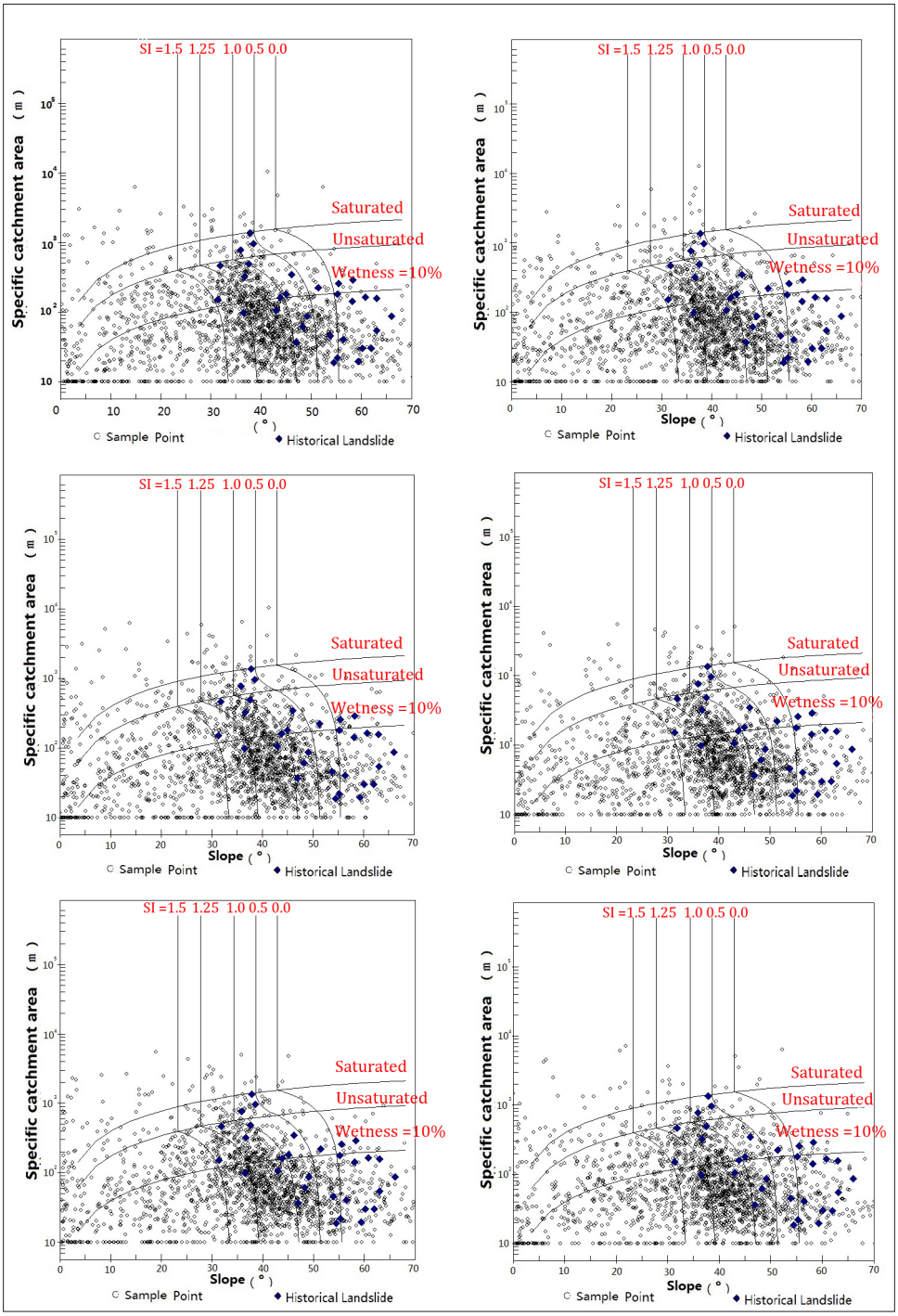

Figure 8 - Scatter plot of the six slope-specific catchment areas.

The slope stability map in Figure 6 contains 1200 × 1889 pixels (length × width for a total of 2,266,800 pixels). This area covers a dimension of 1.2 × 18.9 km (the orientation of the vertical axis is towards the north). Considering the speed of computation and the size of the map, several points were sampled to show the distribution in the study area. The selection ratio was set to 1:1000. Thus, 2000 random points were selected as samples from the entire area, corresponding to 14 sample points per square kilometer, to indicate the distributions of the slope gradients and specific catchments. Figure 8 shows six results for the distribution of randomly selected samples and recent landslides in a slope-specific catchment area scatter plot with sample scattering at different slope stability levels [Reutebuch et al., 2005]. In this plot, the space was split into six SI classes by five lines from left to right with SI steps of 1.5, 1.25, 1.0, 0.5, and 0.0, respectively. Most of the sample points (circle points in Fig. 8) were gathered in the middle of the plot, mainly in classes 3 and 4, at slope angles of 30-55° and with specific catchment areas of 10-1000 m. The positions of previous shallow landslides (blue points in Fig. 8) revealed that most shallow landslides were located in unstable regions (9 on class 3, 4 on class 2, and 13 on class 1). Seventeen landslides occurred at slope angles greater than 35° and in specific catchment areas of less than 1000 m. The lines splitting four horizontal zones (Fig. 8) revealed the following soil water saturation conditions: saturated, unsaturated, and wet (=10%). Most of the random sampling points were unsaturated, and all recent landslides occurred under unsaturated soil conditions. Thus, the results indicated that loose soil textures could trigger landslides during the rainfall-infiltration state before runoff occurs.

Discussion on the influences of ALS data

Influence of point cloud density

Five datasets were derived from the original filtered point cloud by using the following decimation factors: 5, 10, 25, 100, and 200. Then, five new DEM with a spatial resolution of 10 m were derived from such datasets. To analyse the influences of point cloud density on the precision of each DEM, the elevations of those points in the original DEM (Z_i) were used as reference values. The elevations of corresponding points in the decimated DEM (z_i^d, where d refers to the decimation level) were compared with the reference points. The root mean square error (RMSE) was selected as a metric to evaluate the DEM precision as follows:

$$RMSE = \pm\sqrt{\sum_{i=1}^{n} \frac{(z_i - z_i^d)^2}{n}} \quad [6]$$

where n is the number of points.

Slope stability analyses were repeated by applying the SINMAP model to these five datasets after decimation. The precision of slope stability evaluation was evaluated for each dataset with reference to the original data precision. The precision D-value, which is defined as the standard deviation of the slope stability classification between a generic decimated point cloud and the reference point cloud, was also adopted as a metric (Tab. 5).

Table 5 - Result of the accuracy analysis of DEM samples obtained from cloud points with different point densities.

Decimation factors	RMSE (m)	Precision	Precision D-value
5	4.7134	75.00%	6.25%
10	5.402	59.38%	21.87%
25	9.056	53.13%	28.12%
100	16.392	50.00%	31.25%
200	20.311	46.88%	34.37%

When the point cloud density was lower, the RMSE of the corresponding DEM increased and the accuracy of the slope stability evaluation decreased. As shown in Figure 9, the RMSE increased nearly linearly as a function of the decimation factor, indicating that the point cloud density and the DEM accuracy are linearly related. The behaviour of D-value is similar to that of a quadratic curve and shows a clear change in the correspondence of decimation factor 20. Thus, when the point cloud density is high, small density changes may generate large slope stability variations. On the other hand, when the point cloud density is low, the DEM precision is not significantly affected.

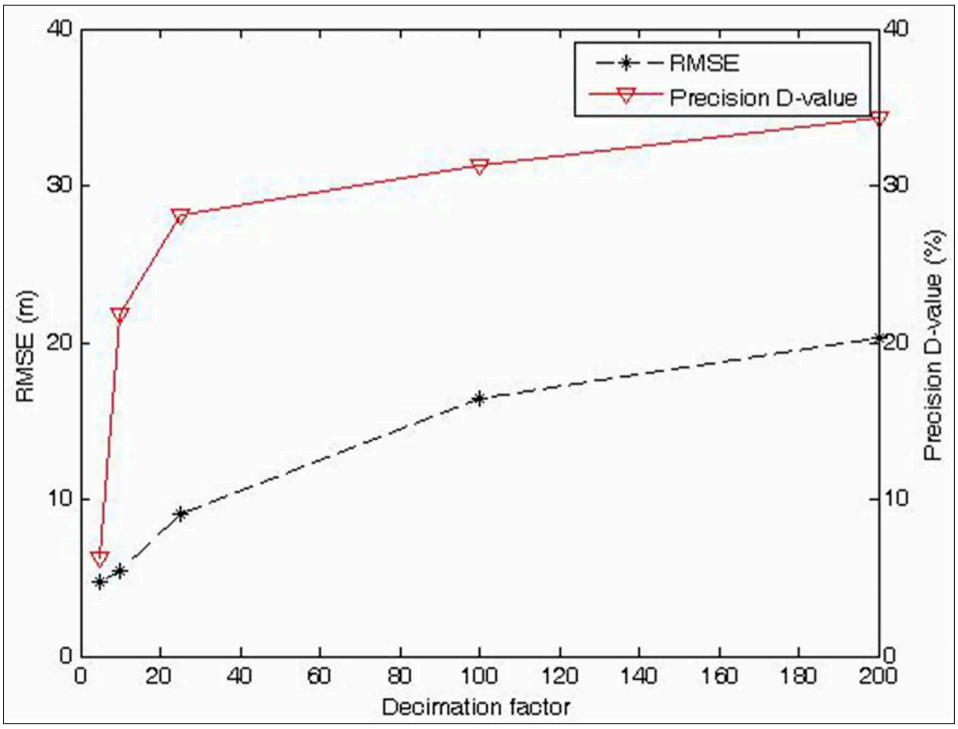

Figure 9 - Results of the RMSE of DEM and the precision D-value at different point cloud densities.

Influence of random errors

Five sets of ALS data were derived from the original laser point cloud. Gaussian distributed noise with s = 2 m was added to the point coordinates to simulate different levels of random errors. As shown in Table 6, Gaussian noise was introduced in the original dataset and in two decimated datasets that were used in the first group of experiments (according to decimation factors 10 and 100, respectively).

Table 6 - Setting five groups of experimental datasets to investigate the effects of adding Gaussian noises.

Dataset number	Decimation scale	Gaussian distributed noise
1	1	Sigma = 2 m
2	10	--
3	10	Sigma = 2 m
4	100	--
5	100	Sigma = 2 m

Next, five DEM samples with the same spatial resolution as the original data were created from all datasets listed in Table 6. By applying the SINMAP model, five slope stability maps were derived for the study area (see Fig. 10). From the slope stability maps in Figure 10, the spatial distributions of the unstable areas featured the same general trends with different point cloud densities and Gaussian noise. However, the extension of unstable regions is different. Table 7 shows the statistical results of the slope stability maps in the case of different datasets. A comparison between the slope stability maps derived from non-corrupted data and from data with Gaussian noise at the same point cloud density was conducted. This result indicates that the unstable regions have always been largely overestimated when applying noisy data. This was confirmed by the statistical results as indicated in Table 7. Regarding the original point density, the total unstable region was 14.43%, which increased to 20.08% when using corrupted data. For the decimated data (factor 10), the non-corrupted data caused an estimated unstable region of 11.95% (dataset 2), while the noisy data brought an estimated unstable region of 19.55% (dataset 3). Similarly, with a decimation factor of 100, an estimated unstable region of 9.29% was obtained from non-noisy data (dataset 4) and an estimated unstable region of 15.31% was obtained from noisy observations (dataset 5). When comparing the precision validated by recent landslides in each group, dataset 4 showed the lowest precision (50.00%). In addition, as shown in Figure 11, the precision decreased as the decimation scale increased. When data at the original point density were used, the precision of the slope stability map based on noisy data was lower than that without added noise. Nevertheless, with the higher decimation factor, the opposite behaviour was observed.

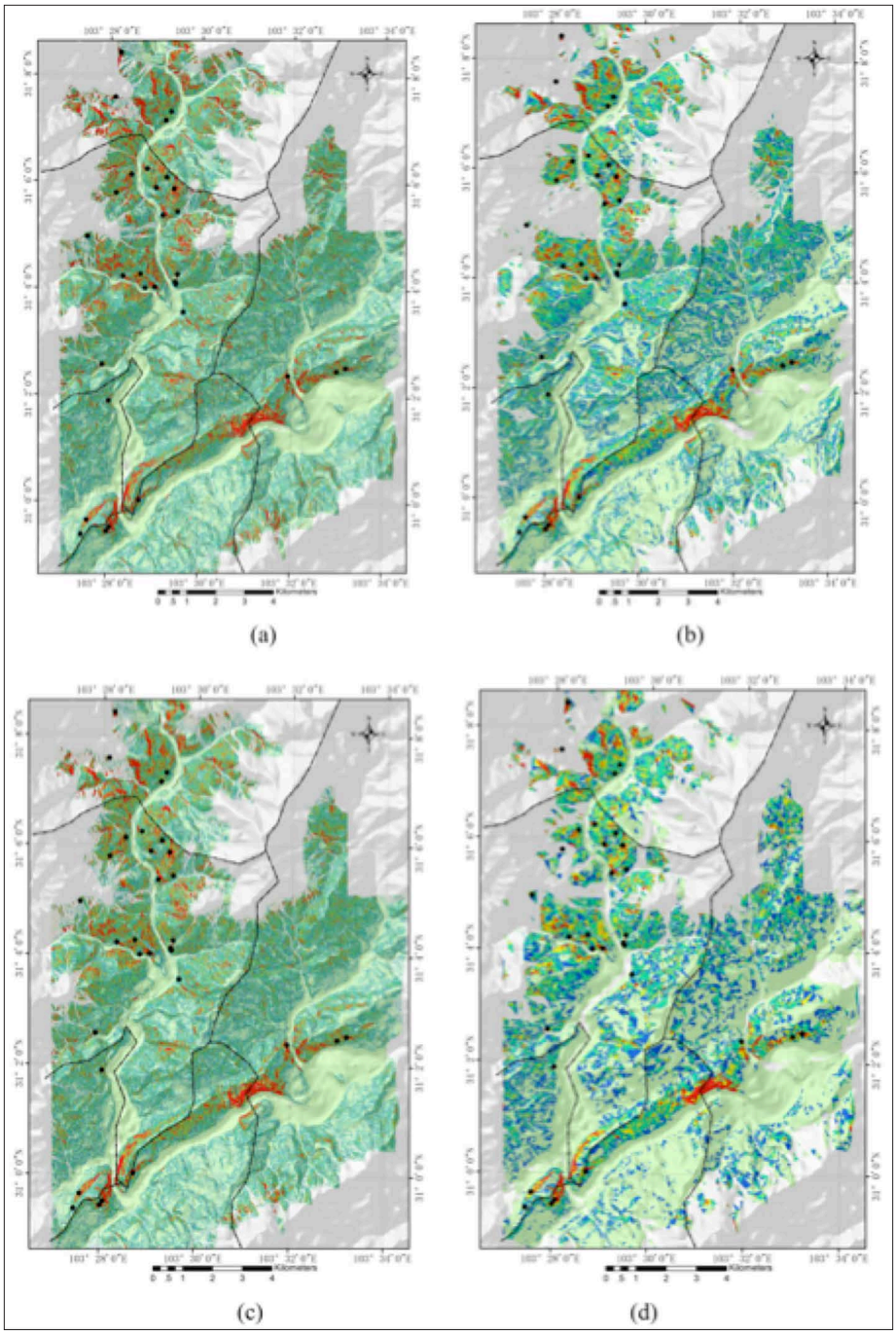

Figure 10 (Continued on the next page) - Slope stability maps obtained from experimental dataset 1(a), 2(b), 3(c), 4(d) and 5(e), and (f) is the classification legend.

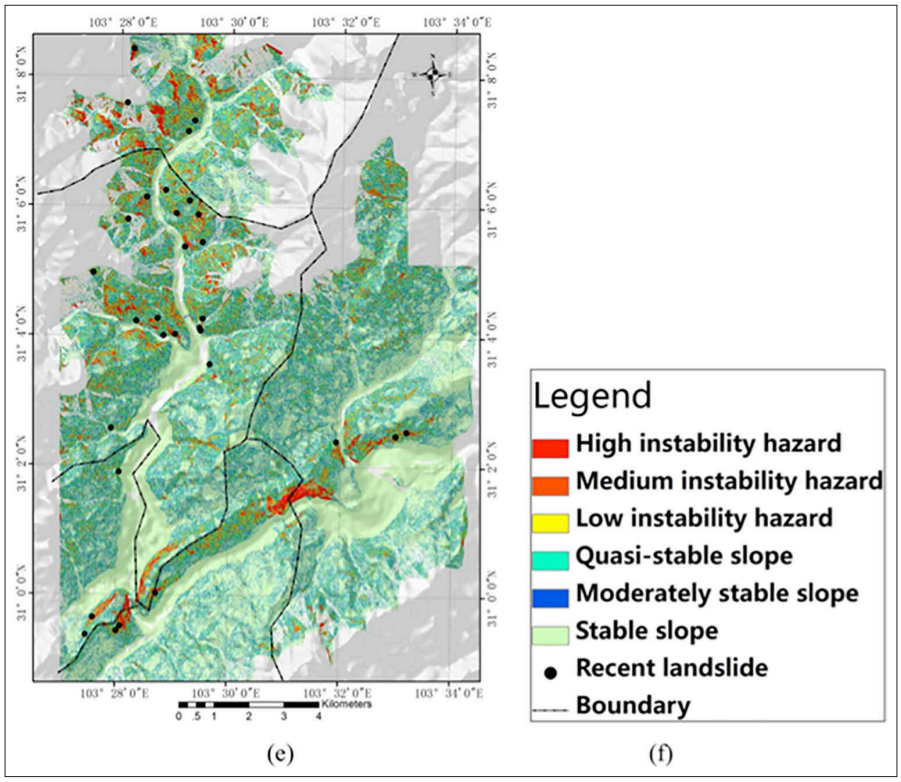

Figure 10 (Continued from preceding page) - Slope stability maps obtained from experimental dataset 1(a), 2(b), 3(c), 4(d) and 5(e), and (f) is the classification legend

The two experiments of point cloud density and random errors indicated that the data quality had a significant effect on the slope stability analysis for the SINMAP model. Particularly, the point cloud density and the adopted point-cloud-filtering algorithm to reduce the effects of noise are two important factors.

Table 7 - Statistical results of slope stability mapping in the case of the original dataset and the datasets 1 to 5.

Dataset number	High instability	Medium instability	Low instability	Quasi-stable slope	Moderately stable slope	Stable slope	Precision
	Area/ landslide number	Area/ landslide number	Area/ landslide number	Area/ landslide number	Area/ landslide number	Area/ landslide number	
Original	2.86%, 13	3.57%, 4	8%, 9	25.27%,4	17.42%, 2	42.88%, 0	81.25%
1	5.30%, 12	5.78%, 3	9%, 10	22.38%, 4	15.11%, 3	41.96%, 0	78.13%
2	2.02%, 10	2.74%, 4	7.19%, 5	23.02%, 8	16.65%, 2	48.37%, 0	59.38%
3	3.61%, 9	5.67%, 6	10.27%, 6	21.80%, 4	15.31%, 1	43.34%, 3	65.63%
4	1.10%, 3	2.11%, 6	5.99%, 7	19.03%, 11	16.05%, 3	55.71%, 0	50.0%
5	2.38%, 7	4.45%, 6	8.48%，5	19.27%, 10	14.81%, 2	50.61%, 1	56.25%

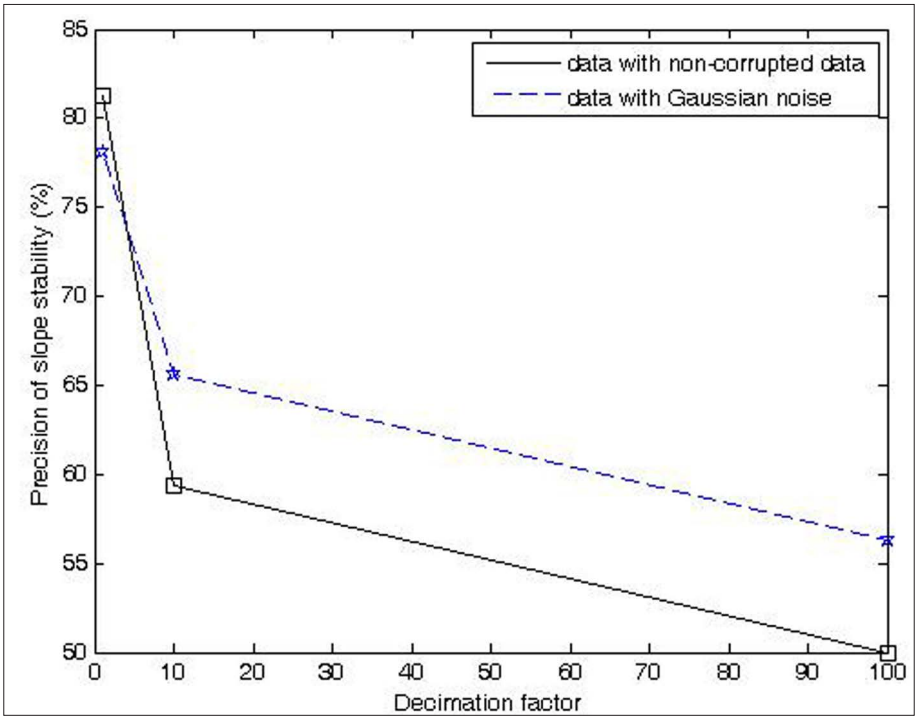

Figure 11 - Precision of slope stability as a function of the decimation factor in the case of data with Gaussian and non-corrupted data.

Conclusion

This study has addressed the application of ALS data for investigating slope stability in the Yingxiu area (Sichuan Province, China), where massive occurrences of shallow landslides were reported after the 2008 Wenchuan Earthquake. A simplified infinite slope stability model, SINMAP, was utilized in this work. The analysis is based on the high precision topography data derived from ALS. Several internal and external factors (*e.g.*, soil texture, terrain lithology and precipitation) were used in the SINMAP model to assess the slope stability in the Yingxiu area. The major advantages of the utilized SINMAP model include its simplicity and the possibility of accommodating uncertain parameters by specifying upper and lower limits based on a uniform probability distribution. This option is proven to be useful in the Yingxiu area because the precision of precipitation data obtained from media and past reports may be insufficient for a dynamic simulation of rainfall, thus possibly introducing significant errors.

The SINMAP model was deployed to classify the slope stability of the Yingxiu area into six different levels. With reference to recent shallow landslide inventory, 81.25% of the previous events were found present in areas that were classified as unstable in this study. By comparing a slope stability map with local residential maps, it appears that most susceptible regions are located in steep slopes and along riversides. In addition, the possible influence of the ALS data quality on the DEM generation has been deeply investigated in this study. In the first group of experiments, the influence of the original ALS point density was tested

by decimated point clouds. Given that an average ALS resolution of 6 points/m^2, the experiments have demonstrated that the derived DEM quality may be very different when a decimation factor is applied. In the second group of experiments, additional Gaussian noise was added to the original point cloud to understand the effects of noise on the estimated slope stability map. In this case, the addition of noise brought a potential overestimation of unstable areas. As a result, the ALS data quality had a large impact on the analysis of slope stability using the SINMAP model. The point cloud density of the original ALS data and the filtering algorithm for mitigating the effects of noise can be identified as two key-elements that need to be carefully controlled.

Further study will focus on broadening the SINMAP functions to integrate different geological parameters and soil factors with multiple dimensions and to possibly evaluate landslide stability at different scales.

Acknowledgements

This work was supported by the National Basic Research Program of China (Project No.2013CB733204 and No.2013CB733203), the National Natural Science Foundation of China (Project No. 41371333 and No. 41671413), the Fundamental Research Funds for the Central Universities (Tongji University) and the Key Laboratory of Mining Spatial Information Technology of NASMG (KLM201309). The authors express deep appreciation to the provider of the ALS data, the Eastdawn Company (http://www.east-dawn.com.cn/).

References

Axelsson P. (2000) - *DEM generation from laser scanner data using adaptive TIN models*. International Archives of Photogrammetry and Remote Sensing, 33 (B4/1; PART 4): 111-118.

Beven K., Lamb R., Quinn P., Romanowicz R., Freer J., Singh V.P. (1995) - *Topmodel*. Computer models of watershed hydrology, pp. 627-668.

Beven K.J., Kirkby M.J. (1979) - *A physically based, variable contributing area model of basin hydrology/Un modèle à base physique de zone d'appel variable de l'hydrologie du bassin versant*. Hydrological Sciences Journal, 24 (1): 43-69. doi: https://doi.org/10.1080/02626667909491834.

Bijukchhen S.M., Prabin K., Megh R.D. (2013) - *A comparative evaluation of heuristic and bivariate statistical modelling for landslide susceptibility mappings in Ghurmi-Dhad Khola, east Nepal.* Arabian Journal of Geosciences, 6 (8): 2727-2743. doi: https://doi.org/10.1007/s12517-012-0569-7.

Carrara A., Cardinali M., Detti R., Guzzetti F., Pasqui V., Reichenbach P. (1991) - *GIS techniques and statistical models in evaluating landslide hazard*. Earth Surface Processes and Landforms, 16 (5): 427-445. doi: https://doi.org/10.1002/esp.3290160505.

Chen Q., Hua G., Hongfu Z. (2011) - *Mapping of Seismic Triggered Landslide through Newmark Method-An Example from Study Area Yingxiu*. Coal Geology of China, 11: 013.

Chigira M., Wu X., Inokuchi T., Wang G. (2010) - *Landslides induced by the 2008 Wenchuan earthquake, Sichuan, China*. Geomorphology, 118 (3): 225-238. doi: https://doi.org/10.1016/j.geomorph.2010.01.003.

Cui P., Chen X.-Q., Zhu Y.-Y., Su F.-H., Wei F.-Q., Han Y.-S., Liu H.-J., Zhuang J.-Q. (2011) - *The Wenchuan earthquake (May 12, 2008), Sichuan province, China, and resulting geohazards*. Natural Hazards, 56 (1): 19-36. doi: https://doi.org/10.1007/s11069-009-9392-1.

Cui P., Zhu Y.-Y., Han Y.-S., Chen X.-Q., Zhuang J.-Q. (2009) - *The 12 May Wenchuan earthquake-induced landslide lakes: distribution and preliminary risk evaluation*. Landslides, 6 (3): 209-223. doi: https://doi.org/10.1007/s10346-009-0160-9.

Deb S.K., El-Kadi A.I. (2009) - *Susceptibility assessment of shallow landslides on Oahu, Hawaii, under extreme-rainfall events*. Geomorphology, 108 (3): 219-233. doi: https://doi.org/10.1016/j.geomorph.2009.01.009.

Dietrich W., Reiss E.R., Hsu M.-L., Montgomery D.R. (1995) - *A process-based model for colluvial soil depth and shallow landsliding using digital elevation data*. Hydrological processes, 9 (3-4): 383-400. doi: https://doi.org/10.1002/hyp.3360090311.

Gorum T., Fan X., van Westen C.J., Huang R.Q., Xu Q., Tang C., Wang G. (2011) - *Distribution pattern of earthquake-induced landslides triggered by the 12 May 2008 Wenchuan earthquake*. Geomorphology, 133 (3): 152-167. doi: https://doi.org/10.1016/j.geomorph.2010.12.030.

Hammond C., Hall D., Miller S., Swetik P. (1992) - *Level I stability analysis (LISA) documentation for version 2.0*. General technical report INT, 285.

Hong Y., He X., Cerato A., Zhang K., Hong Z., Liao Z. (2015) - *Predictability of a Physically Based Model for Rainfall-induced Shallow Landslides: Model Development and Case Studies*. In Modern Technologies for Landslide Monitoring and Prediction, 165-178, Springer.

Jaboyedoff M., Oppikofer T., Abellán A., Derron M.-H., Loye A., Metzger R., Pedrazzini A. (2012) - *Use of LIDAR in landslide investigations: a review*. Natural Hazards 61 (1): 5-28. doi: https://doi.org/10.1007/s11069-010-9634-2.

Kelsey H.M. (1988) - *Formation of inner gorges*. Catena, 15 (5): 433-458. doi: https://doi.org/10.1016/0341-8162(88)90063-X.

Lee S. (2005) - *Application of logistic regression model and its validation for landslide susceptibility mapping using GIS and remote sensing data*. International Journal of Remote Sensing, 26 (7): 1477-1491. doi: https://doi.org/10.1080/01431160412331331012.

Li Z., Shi W., Myint S.W., Lu P., Wang Q. (2016) - *Semi-automated landslide inventory mapping from bitemporal aerial photographs using change detection and level set method*. Remote Sensing of Environment, 175: 215-230. doi: https://doi.org/10.1016/j.rse.2016.01.003.

Lu P., Casagli N., Catani F. (2010) - *PSI-HSR: a new approach for representing Persistent Scatterer Interferometry (PSI) point targets using the hue and saturation scale* International Journal of Remote Sensing, 31 (8): 2189-2196. doi: https://doi.org/10.1080/01431161003636716.

Lu Ping, Stumpf A., Kerle N., Casagli N. (2011) - *Object-oriented change detection for landslide rapid mapping*. IEEE Geoscience and Remote Sensing Letters, 8 (4): 701-705. doi: https://doi.org/10.1109/LGRS.2010.2101045.

Lu P., Casagli N., Catani F., Tofani V. (2012) - *Persistent Scatterers Interferometry Hotspot and Cluster Analysis (PSI-HCA) for detection of extremely slow-moving landslides*

International Journal of Remote Sensing, 33 (2): 466-489. doi: https://doi.org/10.1080/01431161.2010.536185.

Lu P., Catani F., Tofani V, Casagli N. (2014a) - *Quantitative hazard and risk assessment for slow-moving landslides from Persistent Scatterer Interferometry*. Landslides, 11 (4): 685-696. doi: https://doi.org/10.1007/s10346-013-0432-2.

Lu P., Bai S., Casagli N. (2014b) - *Investigating spatial patterns of persistent scatterer interferometry point targets and landslide occurrences in the Arno River Basin*. Remote Sensing, 6 (8): 6817-6843. doi: https://doi.org/10.3390/rs6086817.

Lu P., Wu H., Qiao G., Li W., Scaioni M., Feng T., Liu S., Chen W., Li N., Liu C. (2015a) - *Model test study on monitoring dynamic process of slope failure through spatial sensor network*. Environmental Earth Sciences, 74 (4): 3315-3332. doi: https://doi.org/10.1007/s12665-015-4369-8.

Lu P., Bai S., Casagli N. (2015b) - *Spatial relationships between landslide occurrences and land cover across the Arno river basin (Italy)*. Environmental Earth Sciences, 74 (7): 5541-5555. doi: https://doi.org/10.1007/s12665-015-4569-2.

Lu P., Shang Y. (2015) - *Active Tectonics Revealed by River Profiles along the Puqu Fault*. Water, 7 (4): 1628-1648. doi: https://doi.org/10.3390/w7041628.

Moore I.D., Grayson R.B., Ladson A.R. (1991) - *Digital terrain modelling: a review of hydrological, geomorphological, and biological applications*. Hydrological processes, 5 (1): 3-30. doi: https://doi.org/10.1002/hyp.3360050103.

Moore I.D., O'Loughlin E.M., Burch G.J. (1988) - *A contour-based topographic model for hydrological and ecological applications*. Earth Surface Processes and Landforms, 13 (4): 305-320. doi: https://doi.org/10.1002/esp.3290130404.

O'Loughlin E.M. (1986) - *Prediction of surface saturation zones in natural catchments by topographic analysis*. Water Resources Research, 22 (5): 794-804. doi: https://doi.org/10.1029/WR022i005p00794.

Pack R.T., Tarboton D.G., Goodwin C.N. (1998) - *The SINMAP approach to terrain stability mapping.* Paper presented at the 8th congress of the international association of engineering geology, Vancouver, British Columbia, Canada.

Qiao G., Lu P., Scaioni M., Xu S., Tong X., Feng T., Wu H., Chen W., Tian Y., Wang W. (2013) - *Landslide investigation with remote sensing and sensor network: From susceptibility mapping and scaled-down simulation towards in situ sensor network design*. Remote Sensing, 5 (9): 4319-4346. doi: https://doi.org/10.3390/rs5094319.

Reutebuch S.E., Andersen H.-E., McGaughey R.J. (2005) - *Light detection and ranging (LIDAR): an emerging tool for multiple resource inventory*. Journal of Forestry, 103 (6): 286-292.

Sarkar S., Kanungo D.P. (2004) - *An integrated approach for landslide susceptibility mapping using remote sensing and GIS*. Photogrammetric Engineering & Remote Sensing, 70 (5): 617-625. doi: https://doi.org/10.14358/PERS.70.5.617.

Sekiguchi T., Sato H.P. (2004) - *Mapping of micro topography using airborne laser scanning*. Landslides, 1 (3): 195-202. doi: https://doi.org/10.1007/s10346-004-0021-5.

Tang C., Zhu J., Ding J., Cui X.F., Chen L., Zhang J.S. (2011) - *Catastrophic debris flows triggered by a 14 August 2010 rainfall at the epicenter of the Wenchuan earthquake*. Landslides, 8 (4): 485-497. doi: https://doi.org/10.1007/s10346-011-0269-5.

Terhorst B., Kreja R. (2009) - *Slope stability modelling with SINMAP in a settlement area*

of the Swabian Alb. Landslides, 6 (4): 309-319. doi: https://doi.org/10.1007/s10346-009-0167-2.

Turner D., Lucieer A., de Jong S.M. (2015) - *Time Series Analysis of Landslide Dynamics Using an Unmanned Aerial Vehicle (UAV)*. Remote Sensing, 7 (2): 1736-1757. doi: https://doi.org/10.3390/rs70201736.

Van Western C. (2000) - *The modelling of landslide hazards using GIS*. Surveys in Geophysics, 21 (2): 241-255. doi: https://doi.org/10.1023/A:1006794127521.

Xu C., Xu X. (2013) - *Controlling parameter analyses and hazard mapping for earthquake-triggered landslides: an example from a square region in Beichuan County, Sichuan Province, China*. Arabian Journal of Geosciences, 6 (10): 3827-3839. doi: https://doi.org/10.1007/s12517-012-0646-y.

Xu Q., Fan X.-M., Huang R.-Q., Westen C.V. (2009) - *Landslide dams triggered by the Wenchuan Earthquake, Sichuan Province, south west China*. Bulletin of engineering geology and the environment, 68 (3): 373-386. doi: https://doi.org/10.1007/s10064-009-0214-1.

Yang X., Zhang Y., Hu C., Hao H., Huang Y., Zhou L., Li G., Kong Y., Zheng, Q. (2005) - *The report of geological hazards investigation and regionalization of Wenchuan County of Aba Tibetan and Qiang Autonomous Prefecture of Sichuan Province* (in Chinese) Guanghan Geological Engineering Exploration Institute of Sichuan Province: Internal report.